COMPUTATIONAL ELECTROCHEMISTRY

CASPER H. L. BEENTJES

Mathematical Institute, University of Oxford, Oxford, UK

ABSTRACT. We derive a mathematical model for the dynamics of redox reactions at an electrode-liquid interface when an external potential is applied to the electrode. The model couples chemical transport with electron kinetics and the set-up of the model allows for a general range of external potentials. We further investigate the resulting dynamics of five types of external potential. Numerical simulations are performed using a finite difference and a Chebyshev collocation approach yielding perfect agreement with theory whenever available.

1. INTRODUCTION

Electrons form a key ingredient in many chemical reactions, particularly in the case of redox reactions. This particular type of reaction encompasses a wide range of phenomena. Examples are the corrosion of metals and many important biological reactions, such as the oxidation of glucose, which is used to provide energy to cells.

Electrochemistry concerns the study of such chemical reactions in a typical set-up where there is a redox reaction between a solid electrode and a solute, often dissolved in liquid. Electron transfer can take place when electrons in a chemical have sufficient energy to move from their orbits into lower energy orbits around different molecules. The potential of a chemical determines the energy of its electrons and therefore dictates the electron transfer. This makes the set-up of electrochemistry so beneficial, as it allows one to directly control the potential of the electrode by use of an external power supply. Information about the electron transfer can in turn be accurately acquired by measurement of the current that flows due to the transfer. This way of exploring the dynamics is called amperometry. The specific case where one measures a changing current as a result of an externally applied potential is also known as voltammetry. Many different techniques of voltammetry have been proposed, which all differ in the way they apply the potential on the electrode. For example, a steady potential or a time-dependent potential. Traditional methods such as spectroscopy often fail to capture the electron dynamics because of the size and velocity of the electrons involved. Voltammetry, on the other hand, can yield direct insight into the kinetics of the electron transfer by measurement of the current, which makes it an indispensable tool in analytical chemistry.

This paper studies the mathematical modelling of electrochemical problems. We examine models for five widespread voltammetry types, chronoamperometry, linear sweep voltammetry, cyclic voltammetry, alternating current voltammetry and square wave voltammetry. Firstly we introduce the basics of mathematical modelling of the electrode processes in combination with transport of the chemicals by means of differential equations. Subsequently we analyse the

resulting mathematical models and in some special cases analytical solutions can be found. There is, however, a wider class of voltammetry problems for which exact solutions are as yet unknown and to investigate these, we utilise numerical simulations to find approximate solutions.

2. Mathematical model

We will focus on the problem of a planar electrode as depicted in Figure 1. The assumption is made that the size of the electrode is such that we can neglect the effect of the edges and therefore consider a one-dimensional problem with only the vertical space-coordinate x. We consider two chemical species A and B which can form and react at the surface of the electrode. The model aims to describe the concentrations of the chemicals, $c_A(x,t)$ and $c_B(x,t)$ respectively.
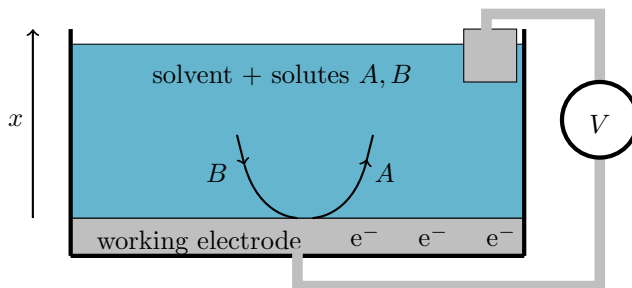

FIGURE 1. Schematic diagram of a planar electrode problem. The working electrode is in contact with a liquid containing some solvent in which the solutes A, B are dissolved. At the electrode surface a reaction of B into A takes place. Note that the contra reaction also occurs if the reaction is reversible, but it is not depicted here. A counter electrode needs to be present to close the electrical circuit.

In experiments the observed results, such as the current, will often reflect only local effects at the electrode. Therefore we assume that the counter electrode is far away from the working electrode, making its influence on the working electrode negligible.

The main processes responsible for change in concentration are the transport of chemicals through the solvent and the reaction of the chemicals at the electrode, which need to be incorporated in the model.

2.1. **Transport of chemicals.** The chemicals A and B can be transported through the liquid by three basic processes, namely diffusion, convection and migration. Here, migration is the effect that charged species will be either repelled or attracted by the electrode surface as we apply a potential. Consequently, the change of concentration would be described by a Nernst-Planck equation, which describes mass conservation for a charged chemical species in a solvent and incorporates all three transport types.

For reasons of simplicity we will, however, consider a more elementary problem where we neglect effects of migration and convection. This can be achieved experimentally as well. To neglect the convection effects we can consider an unstirred solution over a short time so that there is no natural convection due to temperature or external convection of the chemicals. The migration is often excluded from experiments by adding an auxiliary electrolyte to the liquid, which does not react or influence reactions at the electrode surface. This results in an effective screening of the potential gradient induced by the electrode and therefore makes the migration of A and B negligible.

The Nernst-Planck equation now reduces to Fick's second law describing the transport of mass purely due to diffusion

$$
(1) \qquad
\begin{cases}
\dfrac{\partial c_A}{\partial t} &= D_A \dfrac{\partial^2 c_A}{\partial x^2}, \\[2mm]
\dfrac{\partial c_B}{\partial t} &= D_B \dfrac{\partial^2 c_B}{\partial x^2},
\end{cases}
$$

where $D_{A,B}$ is a diffusion coefficient and it can possibly be different for both species.

This gives PDEs for c_A and c_B, which need to be supplemented by suitable initial conditions and four boundary conditions to close the system. We assume that initially we have a homogeneous solution of purely A with bulk concentration c_{bulk}, i.e.

$$
(2) \qquad
\begin{cases}
c_A(x,0) &= c_{\text{bulk}}, \\
c_B(x,0) &= 0.
\end{cases}
$$

Now assume that the vertical direction is sufficiently large, i.e. the volume of the chemical cell is large. Furthermore recall that in order to neglect convection we had to consider the problem on a small enough timescale. We then view the chemical cell as a semi-infinite domain, where at large distances from the electrode the concentrations are undisturbed by the electrode and thus remain at the bulk values. This gives the far-field boundary conditions

$$
(3) \qquad
\begin{cases}
c_A(x,t) &\to c_{\text{bulk}} \\
c_B(x,t) &\to 0
\end{cases}
\qquad \text{as } x \to \infty, \ t > 0.
$$

Two more boundary conditions are needed and they are prescribed at the electrode-liquid interface. The first one follows from the conservation of mass at the surface. If we use Fick's first law, giving the flux of a diffusing chemical, we find that

$$
(4) \qquad D_A \frac{\partial c_A}{\partial x} + D_B \frac{\partial c_B}{\partial x} = 0 \qquad \text{at } x = 0, \ t > 0.
$$

The last boundary condition will depend on the applied potential at the electrode resulting in redox reactions.

2.2. **Electron transfer and current.** We will consider a reductant-oxidant couple A, B reacting in a redox reaction at the electrode surface

$$
(5) \qquad A \ \underset{k_{\text{red}}}{\overset{k_{\text{ox}}}{\rightleftharpoons}} \ B + ne^-,
$$
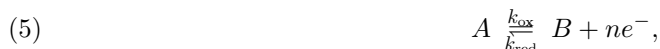
where k_{red} and k_{ox} are the reaction rates of both reactions. The total current I at the electrode due to the redox reaction (5) is directly related to the flux of the chemicals at the surface by Faraday's law of electrolysis

$$
(6) \qquad I = nF\mathcal{A}D_A \left. \frac{\partial c_A}{\partial x} \right|_{x=0},
$$

where $\mathcal{A}$ is the surface area of the working electrode and F is the Faraday constant.

Note that the current involves the flux of molecules A at the electrode-liquid interface. The chemicals will react following (5) and often this reaction can be modelled as a first-order reaction. In that case the rate-law equation at the surface gives a reaction flux of A. If we combine this with Fick's first law for the diffusion flux and demand that there is no net-flux of A through the electrode we find the remaining boundary condition

$$
(7) \qquad D_A \frac{\partial c_A}{\partial x} = k_{\text{ox}} c_A - k_{\text{red}} c_B, \qquad \text{at } x = 0.
$$

There are however two remaining unknowns in equation (7), the reaction rates. A widely used empirical model for the reaction rates is the Arrhenius equation

$$(8) \qquad\qquad k = K \exp\left(-\frac{\Delta G^{\ddagger}}{RT}\right),$$

where R is the universal gas constant, T the temperature and $\Delta G^{\ddagger}$ is the activation Gibbs free energy. As the potential of the electrode, denoted by E, controls the energy of the electrons on the working electrode it is expected that this will influence the Gibbs free energy $\Delta G^{\ddagger}(E)$. Decreasing the potential of the electrode will move the electrons on the electrode to a higher energy level. This stimulates the uptake of electrons by the oxidant A, thus lowering $\Delta G^{\ddagger}_{\mathrm{red}}$ and increasing $\Delta G^{\ddagger}_{\mathrm{ox}}$. An opposite effect is expected if we ramp up the potential. Empirical models have indeed been proposed for $\Delta G^{\ddagger}$ and arguably the most simple relation, a linear relation, is given by the Butler-Volmer model [2, 5]

$$(9a) \qquad\qquad \Delta G^{\ddagger}_{\mathrm{red}} = \Delta G^{\ddagger}_0 + \alpha nF(E - E^0_f),$$
$$(9b) \qquad\qquad \Delta G^{\ddagger}_{\mathrm{ox}} = \Delta G^{\ddagger}_0 - (1-\alpha)nF(E - E^0_f),$$

where $\alpha \in [0,1]$ is the charge transfer coefficient and E^0_f is the formal potential. At the formal potential the rates of both equations are equal. The charge transfer coefficient reflects the symmetry in the effect of the potential on the energy barrier. Often a value of $\alpha = 1/2$ is taken, reflecting a symmetric effect of E on the barrier.

The boundary condition (7) together with the Butler-Volmer kinetics becomes now at $x = 0$

$$(10) \qquad D_A \frac{\partial c_A}{\partial x} = K_0 \left(c_A \exp\left\{ (1-\alpha)\frac{nF(E - E^0_f)}{RT} \right\} - c_B \exp\left\{ -\alpha\frac{nF(E - E^0_f)}{RT} \right\} \right),$$

where K_0 is the reaction rate constant at the formal potential. This reaction rate is a measure for the reversibility of the reaction at the reaction surface. For high K_0 the redox reactions will be fast and the chemicals will establish an equilibrium at the electrode surface, the reaction is said to be reversible. For low K_0, on the other hand, the electron transfer rate is slow and the chemicals cannot sustain an equilibrium, these reactions are known as quasi-reversible reactions.

This completes the model for the chemical dynamics; two governing PDEs (1) with initial conditions (2) and boundary conditions (3,4,10).

2.3. **Non-dimensionalisation.** To keep analysis tractable we non-dimensionalise the model by using the following dimensionless quantities

$$(11a) \qquad\qquad a = \frac{c_A}{c_{\mathrm{bulk}}}, \quad b = \frac{c_B}{c_{\mathrm{bulk}}}, \quad d = \frac{D_B}{D_A}, \quad \hat{x} = \frac{x}{L}, \quad \hat{t} = \frac{D_A t}{L^2}$$

$$(11b) \qquad\qquad \hat{I} = \frac{L}{nF A D_A c_{\mathrm{bulk}}} I, \quad \theta = \frac{nF}{RT}(E - E^0_f), \quad k_0 = \frac{L}{D_A} K_0.$$

This results in the following non-dimensional system of equations with initial and boundary conditions which will be considered in this paper

(12a) $\qquad a_t = a_{xx} \quad$ for $x > 0$, $t > 0$,

(12b) $\qquad b_t = db_{xx} \quad$ for $x > 0$, $t > 0$,

(12c) $\qquad a(x, 0) = 1, \quad b(x, 0) = 0$,

(12d) $\qquad a(x, t) \to 1, \quad b(x, t) \to 0 \quad$ as $x \to \infty$, $t > 0$,

(12e) $\qquad a_x(0, t) + db_x(0, t) = 0 \quad$ for $t > 0$,

(12f) $\qquad a_x(0, t) = k_0 \left[a(0, t)e^{(1-\alpha)\theta} - b(0, t)e^{-\alpha\theta} \right] \quad$ for $t > 0$,

(12g) $\qquad I(t) = a_x(0, t)$.

3. Numerical methods

As mentioned earlier, analytical progress on the formulated system cannot always be expected, which is mainly due to the boundary conditions. Therefore we often use numerical methods to explore the model dynamics. In this paper we use the method of lines [8]. We convert the PDEs to a system of ODEs by first discretising the PDEs in the spatial direction. This replaces the continuous $a(x, t)$ by a vector $\mathbf{a}(t) = [a_1(t), \ldots, a_m(t)]$ defined on a discrete grid with m points $\{x_j\}_{j=1}^m$, such that $a(x_j, t) \approx a_j(t)$. A similar transformation is applied to $b(x, t)$. By discretising in the spatial direction we must replace the continuous (linear) diffusion operators in (12a, 12b) with linear operators, i.e. matrices, on $\mathbf{a}(t)$ and $\mathbf{b}(t)$. We will denote this as a generic matrix $\mathbf{D}_2$, the second order differentiation matrix. The result is an ODE system, with the approximation of (12a)

$$(13) \qquad \frac{d\mathbf{a}(t)}{dt} = \mathbf{D}_2\mathbf{a}(t).$$

The equation for $\mathbf{b}(t)$ is the same except for the factor d. The boundary conditions and initial conditions are applied pointwise. This ODE-system is then solved along lines of constant position, hence the method of lines, using a suitable ODE integration scheme.

3.1. **Spatial discretisation.** Two different approaches are followed for the spatial discretisation, reflecting a different choice of grid points $\{x_j\}_{j=1}^m$. Note that the continuum spatial domain is $[0, \infty)$, but numerically this is not feasible as we need to work with a finite number of spatial points. Therefore we will truncate the domain for some sufficiently large $x = x^*$. We assume that the electrode process does not influence the solution at $x > x^*$ and set $a(x^*, t) = 1$ and $b(x^*, t) = 0$, the bulk values.

3.1.1. *Finite differences.* An widespread approach is the method of finite differences, which makes use of an equispaced grid with grid-spacing Δx. To approximate the second space-derivative we employ a Taylor approximation of $a(x_j, t)$ to find the central difference approximation

$$(14) \qquad a_{xx}(x_j, t) \approx \frac{a_{j+1}(t) - 2a_j(t) + a_{j-1}(t)}{(\Delta x)^2}.$$

The error in this approximation is $\mathcal{O}((\Delta x)^2)$. From this we find the diffusion matrix

$$(15) \qquad \mathbf{D}_2 = \frac{1}{(\Delta x)^2} \begin{pmatrix} -2 & 1 & & \\ 1 & -2 & \ddots & \\ & \ddots & \ddots & 1 \\ & & 1 & -2 \end{pmatrix}.$$

Note that we still need to take care of the boundary conditions and that we are interested in the current. The far-field boundary conditions are Dirichlet boundary conditions in the truncated domain and can be pointwise imposed at the last gridpoint. The situation at the electrode is, however, more cumbersome as the boundary conditions are of Neumann and Robin type. A central difference approximation is not possible, as we are at the boundary of the grid. We choose to employ a forward difference formula of second-order, so that the error order matches that of the diffusion operator. This yields

$$(16) \qquad a_x(0, t) \approx \frac{-3a_1(t) + 4a_2(t) - a_3(t)}{2\Delta x},$$

and similar formulation for $b_x(0, t)$. One of the main advantages of this method, as we shall see in time-stepping of the ODE, is that the differentiation matrix has a sparsity pattern. The pattern will be modified at the first and last row due to the boundary conditions, but the matrix remains sparse. A possible downside is the convergence of the method, which is predicted to be of geometric order in space, second order to be more precise. The number of gridpoints $N = \mathcal{O}((\Delta x)^{-1})$ and convergence is thus $\mathcal{O}(N^{-2})$. Resultantly N needs to increase by a fair amount to gain more accuracy.

3.1.2. *Chebyshev collocation.* If the function we are approximating is smooth we can construct a method which has better convergence properties, a spectral method [10]. The convergence is of the order $\mathcal{O}(N^{-m})$ for any $m > 0$. This spectral convergence is significantly better than the convergence for finite difference which has a fixed $m > 0$. Therefore this method can use far fewer points to obtain higher accuracy.

The main idea is that we expand our solution on a set of carefully chosen basis functions. As we have non-periodic boundary conditions we can use Chebyshev polynomials as basis functions for the spectral method. The spatial grid is a corresponding non-uniform Chebyshev grid. The gain in convergence comes from the fact that we use global approximation of the function instead of the local approximation as before. This global approximation of the function over the grid at every point has the side-effect that the differentiation matrix will be a full matrix $\mathbf{D}_2$. To find the current and first-derivatives at the electrode surface we use a global Chebyshev approximation of the derivative, just as we approximated the second derivative globally. We trade sparsity for a much lower number of grid-points compared to finite differences.

A positive side-effect of the use of Chebyshev collocation is the grid density near the electrode surface. As the Chebyshev grid is non-uniform, with a higher density towards the boundary of the domains, we have more resolution close to the electrode. We expect that most of the dynamics will happen at the electrode. Therefore a more dense grid near the part of the domain were we expect to see changes is likely to outperform a uniform grid. One could, of course, also find other ways to refine the grid close to the boundary. For example by using a previously discussed finite difference approach in combination with an expanding mesh, c.f. Gavaghan & Bond [6]. These methods, however, do not obtain spectral convergence as they are still based upon finite differences.

3.2. **Time-stepping.** A first note must be made on the coupling between a and b through the boundary conditions at the electrode (12e,12f). Consequently we need to solve for $\mathbf{a}$ and $\mathbf{b}$ simultaneously. In order to approximate a solution to the ODE system governing the concentrations we discretise the solution in time. We look for approximations $\mathbf{a}^i$ at $\{t_i\}_{i=0}^n$, with $t_0 = 0$ and $t_n = T_{\max}$ such that $a(x_j, t_i) \approx a_j^i$. We assume the temporal points are equispaced with spacing Δt and thus $t_j = j\Delta t$. Different methods can be used to discretise the time-derivative resulting in an (algebraic) system of the form

$$(17) \qquad \mathbf{a}^{i+1} = \mathbf{F}(\mathbf{a}^i).$$

Care must be taken as to what kind of integration scheme is used as the diffusion matrix $\mathbf{D}_2$ is ill-conditioned for both spatial discretisations. In fact $\kappa(\mathbf{D}_2) = \mathcal{O}(N^m)$, with $m = 2$ for finite differences and $m = 4$ for the spectral method. In order for the time integration to be stable we therefore use an implicit method in order to prevent severe constraints on the stepsize Δt due to the ill-conditioning of $\mathbf{D}_2$. In this paper we use the first order implicit Euler method to approximate the time derivative at t_{i+1} by

$$\text{(18)} \qquad \frac{d\mathbf{a}(t_{i+1})}{dt} \approx \frac{\mathbf{a}^{i+1} - \mathbf{a}^i}{\Delta t},$$

with first order error $\mathcal{O}((\Delta t)^{-1})$.

If we define $\mathbf{C} = [\mathbf{a}, \mathbf{b}]^T$, we can formulate our numerical discretisation of our model as

$$\text{(19)} \qquad \left(I - \Delta t \begin{pmatrix} 1 & 0 \\ 0 & d \end{pmatrix} \otimes \mathbf{D}_2 \right) \mathbf{C}^{i+1} = \mathbf{C}^i$$

for all points at the interior of the domain. We have to impose the boundary conditions at the same time. This is achieved by imposing (19) on the interior domain points and using the remaining degrees of freedom at the boundary points in the algebraic system of equations to explicitly impose the boundary conditions. In practice this is done by replacing the equations governing the diffusion at the endpoints by explicit discretisations of the boundary conditions. This yields a closed $2m$-system of equations, which by solving for $\mathbf{C}^{i+1}$ lets us march through time. The theoretical convergence rates are observed to hold in practical simulations (see appendix A.1).

4. Voltammetry

We consider different types of voltammetry, all reflecting a specific way to specify the potential as a function of time, i.e. $\theta(t)$ in the dimensionless model.

4.1. Chronoamperometry.
We consider a reversible reaction at the electron surface, i.e. $k_0 \gg 1$, such that (12e) becomes

$$\text{(20)} \qquad \frac{a(0,t)}{b(0,t)} = e^{-\theta},$$

which is the Nernst-equation in non-dimensional form, describing a perfectly reversible redox reaction in absence of diffusion flux. We now assume that initially θ is such that no electron transfer takes place and then ramp up the voltage instantaneously at $t = 0$, $\theta(t) = \Theta H(t)$, where H is the Heaviside step function and Θ the step-height of the potential.

4.1.1. *Analytical solution.*
This problem now admits an exact solution which can be found by looking for a similarity solution in the variable $\eta = x/\sqrt{t}$. If we solve on $x \in [0, \infty)$ we find that

$$\text{(21a)} \qquad a(x,t) = \frac{\sqrt{d}e^\theta}{\sqrt{d}e^\theta + 1} \cdot \mathrm{erf}\left(x/2\sqrt{t}\right) + \frac{1}{\sqrt{d}e^\theta + 1},$$

$$\text{(21b)} \qquad b(x,t) = \frac{e^\theta}{\sqrt{d}e^\theta + 1} \left(1 - \mathrm{erf}\left(x/2\sqrt{t}\right)\right).$$

Upon a differentiation with respect to x this yields the current

$$\text{(22)} \qquad I(t) = \frac{\sqrt{d}e^\theta}{\sqrt{d}e^\theta + 1} \cdot \frac{1}{\sqrt{\pi t}}.$$

It is more insightful to consider the case of $\Theta \gg 1$ so that we derive the more classical chronoamperometry problem where at the electrode surface $a(0,t) = 0$, i.e. the potential is such that all

A gets converted to B. Doing so we arrive at the Cotrell-equations for the chronoamperometry problem

$$\text{(23a)} \qquad\qquad a(x,t) = \text{erf}(x/2\sqrt{t}),$$

$$\text{(23b)} \qquad\qquad b(x,t) = \frac{1}{\sqrt{d}}\left(1 - \text{erf}(x/2\sqrt{dt})\right),$$

$$\text{(23c)} \qquad\qquad I(t) = \frac{1}{\sqrt{\pi t}}.$$

Note that there is an inconsistency between the initial data provided by (12c) and the boundary condition given by the Nernst-equation (20). Furthermore the current starts at zero at $t = 0$ and has a discontinuity as we instantaneously increase the potential.

4.1.2. *Numerical solution.* Numerically we need to consider a finite domain and thus $x^* < \infty$. In view of tractability we only treat the case of complete conversion of A so that we can use the Cotrell-equations as a reference. We have three Dirichlet boundary conditions and one Neumann boundary condition which are implemented as mentioned in (3.2).

We can now observe that the error in a that is made by truncating the domain for the exact solution is expected to be of order $1 - \text{erf}(x^*/2\sqrt{t})$ (based on the difference at x^*), with a similar expression available for b. We therefore choose x^* such that the error by truncating the domain is smaller than the error made by the numerical scheme, as in that case the truncation is not numerically noticeable.
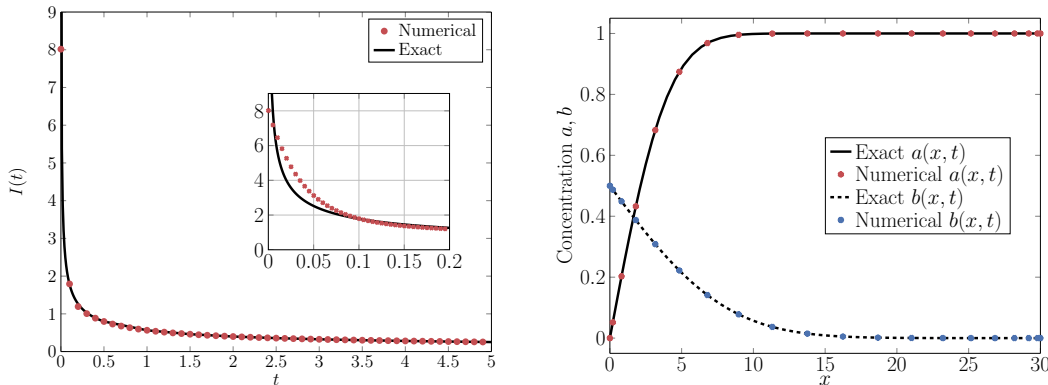
(A) Chronoamperometry current as a function of time. Numerical solution is plotted after every 50 timesteps.

(B) Concentration profiles of a and b at $t = 5$ with $d = 4$.

FIGURE 2. Plot of the current and the concentrations for a chronoamperometry problem with $d = 4$. For the spatial discretisation a Chebyshev collocation with $N = 20$ is used and the timestep is $\Delta t = 10^{-4}$. The inset for the current shows a close-up of the results for small t.

Results of a numerical simulation with Chebyshev collocation are shown in Figure 2. We observe a very good agreement in concentration between the exact solution and the numerics. The numerical current appears to coincide with the Cotrell-equations as well. Note, however, that in Figure 2a the inset shows fair deviations from the exact solution for small t. This is due to the inconsistency between the initial data and the boundary data and the singularity in $I(t)$. This results in a boundary layer-like solution close to the electrode for small t. In order to increasingly distinguish this effect we need to have an increasing number of points close to

the boundary. The effects of this initial inconsistency seem to disappear as t increases, which is comforting, as in experiments one is often interested in the longer term behaviour of the current.

4.2. **Linear sweep voltammetry.** We return to a general k_0 and consider now a linear increase in potential, called a linear sweep voltammetry (LSV). We choose a starting potential θ_0 such that we have very few electron transfers occurring. Therefore we need $k_{\mathrm{ox}} \ll 1$ at $t = 0$ as we start out with purely A and thus $\theta_0 < 0$. This yields

$$(24) \qquad \theta(t) = \theta_0 + t.$$

Some authors prefer to introduce a scan rate ν for the potential, i.e. $\theta(t) = \theta_0 + \nu t$, c.f. [3]. This is, however, in some sense redundant. We can use a remaining degree of freedom in the non-dimensionalisation of space as the problem doesn't prescribe L in any natural way. If we therefore introduce the new length scale $l = \sqrt{\nu}L$ and use this to non-dimensionalise, the factor ν will drop out of the equations and we recover (24). Note that this yields the same dependence of the current on the scan rate, $I \propto \sqrt{\nu}$, as used in the Randles-Ševčík equation [3]. This relation is used experimentally to determine the reaction and diffusion constants by variation of the scan rate.

4.2.1. *Semi-analytics for the current.* Analytical expressions for the solution cannot be easily derived in closed form for the general LSV problem. Nonetheless, if we again consider a reversible reaction, $k_0 \gg 1$, some progress can be made. In this case we observed that (12e) reduces to the Nernst-equation (20). We can then derive an implicit relation for the current $I(t)$ using a Laplace transform in time (see appendix A.3)

$$(25) \qquad F(t) = \frac{\sqrt{d\pi}}{\sqrt{d} + e^{-\theta(t)}} = \int_0^t \frac{I(\tau)}{\sqrt{t-\tau}}\, \mathrm{d}\tau.$$

Note that this expression does not depend on the specific form of $\theta(t)$ and is thus valid for general voltammetry types. One can note that the integrand diverges at $\tau = t$, the edge of the integration domain. This, however, does not necessarily mean that the integral diverges, for example $\int_0^1 \log(x)\, \mathrm{d}x = -1$.

4.2.2. *Numerical solution.* The numerical solution of the concentrations is in essence the same as for the chronoamperometry problem, only replacing a Dirichlet boundary condition by a Robin boundary condition.

A difference with chronoamperometry, however, is that we cannot provide an analytical solution for the concentrations to the problem due to a time-dependent potential. On the other hand we still have an explicit expression for the current in case of $k_0 \gg 1$, which we can use to compare with the numerical results. To effectively use this implicit integral equation for the current, we approximate the integral numerically to find $I(t)$. As noted before the integrand diverges at $t = \tau$ and this proves to be numerically difficult. Therefore we first reformulate the integral equation by either partial integration or by an extra integration (see appendix A.3.1)

$$(26\mathrm{a}) \qquad F(t) = 2\int_0^t I'(\tau)\sqrt{t-\tau}\, \mathrm{d}\tau,$$

$$(26\mathrm{b}) \qquad G(t) = \int_0^t F(s)\, \mathrm{d}s = 2\int_0^t I(\tau)\sqrt{t-\tau}\, \mathrm{d}\tau.$$

The crux of the approximation of the current lies in the following observation

$$(27) \qquad F(n\Delta t) = 2\int_0^{n\Delta t} I'(\tau)\sqrt{n\Delta t - \tau}\, \mathrm{d}\tau = 2\sum_{i=0}^{n-1}\int_{i\Delta t}^{(i+1)\Delta t} I'(\tau)\sqrt{n\Delta t - \tau}\, \mathrm{d}\tau.$$

A similar observation can be made for $G(t)$ in (26b). By using the notation $I_i = I(t_i)$ we then approximate the integrals over (t_i, t_{i+1}), which for a certain class of approximations (see appendix A.3.1 for more details) yields a general form

$$(28) \qquad \int_{t_i}^{t_{i+1}} I'(\tau)\sqrt{n\Delta t - \tau}\,d\tau \approx p_i\,(I_{i+1} - I_i)\,\sqrt{\Delta t},$$

where the constants p_i depend on the particular form of approximation used. This can be used to find an approximation to $I(t_n)$

$$(29) \qquad I_n \approx \frac{1}{p_{n-1}}\left(\frac{F(n\Delta t)}{2\sqrt{\Delta t}} + p_0 I_0 - \sum_{i=1}^{n-1}(p_{i-1} - p_i)I_i\right).$$

The measured currents in voltammetry are often displayed in a voltammogram, a plot of the current versus the applied potential. Since the potential in this case is simply a shifted version of time this is equivalent to an I-t plot.

(A) LSV voltammogram for various k_0. (B) LSV voltammogram for various α.
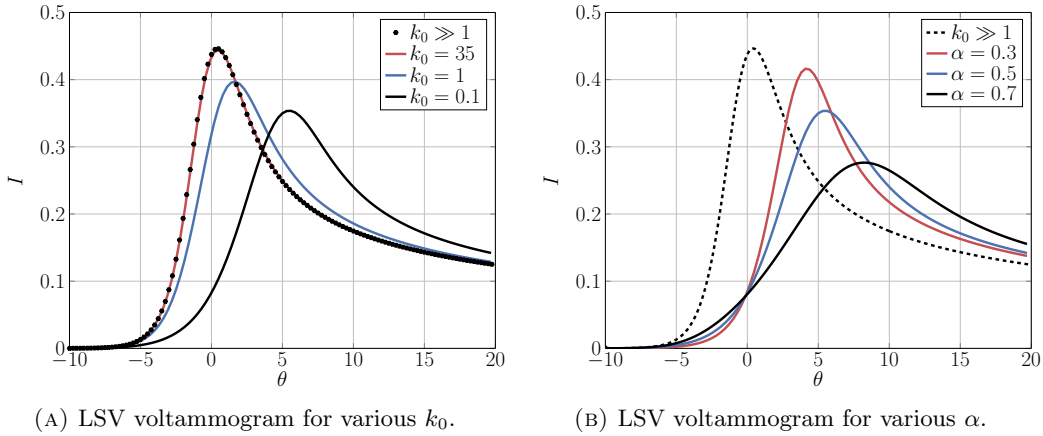
FIGURE 3. Voltammogram for LSV with $d = 4$. The plots show the variation of the current as we vary the parameters in the Butler-Volmer model, the reaction rate k_0 in Figure 3a and symmetry parameter α in Figure 3b. The asymptotic formula for reversible reactions (25) is depicted in both plots as $k_0 \gg 1$. For the spatial discretisation a Chebyshev collocation with $N = 20$ is used and the timestep is $\Delta t = 10^{-4}$.

It is clear from (25) that I does not depend on α for reversible reactions. For non-reversible reactions the effect of α on the current is depicted in Figure 3b. The symmetry factor is a measure of the effect that the external potential has on the Gibbs activation energy. The observations are in agreement with this interpretation as a higher α results in a current that starts increasing for smaller θ, the activation barrier is more effectively lowered.

LSV can be used to look at the reversibility of the equation, as can be seen in Figure 3a. The asymptotic formula (25) derived on the assumption of $k_0 \gg 1$ agrees with the numerical solution for already a moderate value of $k_0 = 35$, with agreement even getting better if we increase k_0. The height and position of the peak of the current shift if we decrease the reaction rate.

4.3. **Cyclic voltammetry.** A voltammetry type very similar to LSV is the cyclic voltammetry (CV). This uses forward and backward linear sweeps to create a triangle wave in time. The

potential for one forward and backward sweep is given by

$$(30) \qquad \theta(t) = \begin{cases} \theta_0 + t, & \text{for } 0 \leq t < \tau_{\text{switch}}, \\ \theta_0 + 2\tau_{\text{switch}} - t, & \text{for } \tau_{\text{switch}} \leq t < 2\tau_{\text{switch}}. \end{cases}$$

This method is popular for its ability to investigate the reaction kinetics as well as the reaction mechanisms. If, for example, we have more than one reaction, or more sophisticated reactions than (5) at the electrode surface, then CV allows one to look at the mechanism of these reactions in separate sweeps [3].

4.3.1. *Numerical solution.* The numerical simulation does not differ from the LSV case as might be expected from the specific form of the potential. We can again use the asymptotic integral formula for the current (25) in the case of a reversible reaction.

The effect of the reversibility of the reaction on a CV is shown in Figure 4. Quasi-reversible reactions cannot attain an equilibrium within the forward sweep, resulting in a qualitatively different voltammogram. The full value of CV, however, is in its use for distinguishing more complex reaction kinetics involving multiple reactions. This is outside the scope of this paper and we refer the interested reader to [3].
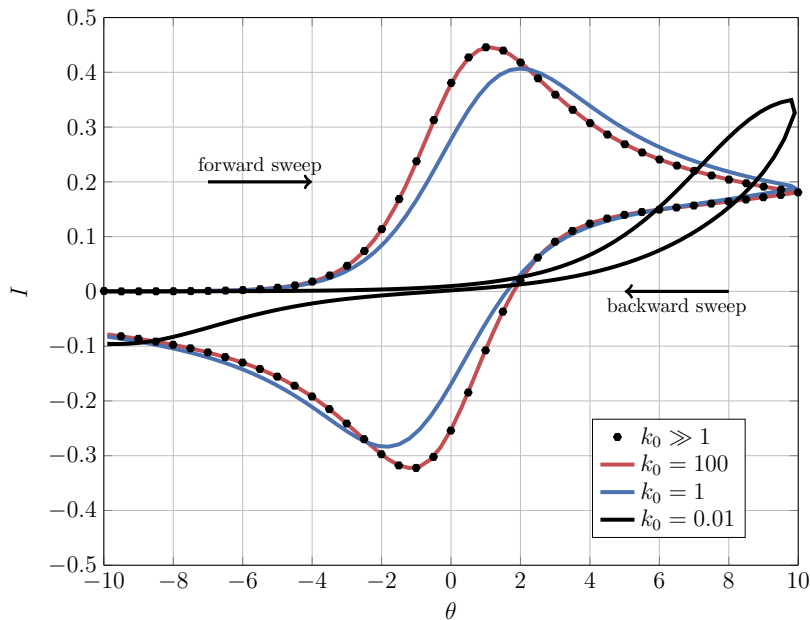

FIGURE 4. Voltammogram for CV with $d = 1$. The plots show the variation of the current as we vary the reversibility of the reaction measured by k_0. The asymptotic formula for reversible reactions (25) is depicted in both plots as $k_0 \gg 1$. For the spatial discretisation a Chebyshev collocation with $N = 20$ is used and the timestep is $\Delta t = 10^{-4}$.

4.4. **Alternating current voltammetry.** Although the previous described methods have proved to be effective methods in general, there exist situations were they lack accuracy [1]. For example in the case of a low concentration of auxiliary electrolyte the effects of a capacitive electric double layer at the electrode start to interfere with the current due to the electrode reactions, the latter known as the Faradaic current. An improved technique to acquire higher quantitative accuracy

is the use of alternating current voltammetry (ACV). This technique imposes a sinusoidal perturbation to the potential. ACV induces phase shifts in the current depending on the origin of the current (i.e. capacitive or Faradaic) which can be used to filter for the desired information.

Here we will only consider the linear ACV, where the potential satisfies

$$(31) \qquad \theta(t) = \theta_0 + t + \Delta\theta \sin(\omega t),$$

where $\Delta\theta$ controls the ac amplitude and ω the ac frequency. The result and numerical analysis carry over in a trivial way to cyclic ACV, which will not be discussed here for that reason.

4.4.1. *Results alternating current component.* The main difference between the direct current and alternating current variants of LSV is the ac component of the resulting current. We can filter this component out of the full current by either a Fourier transform of the signal or via subtraction of the background signal (with $\Delta\theta = 0$), which is the method used in this paper.
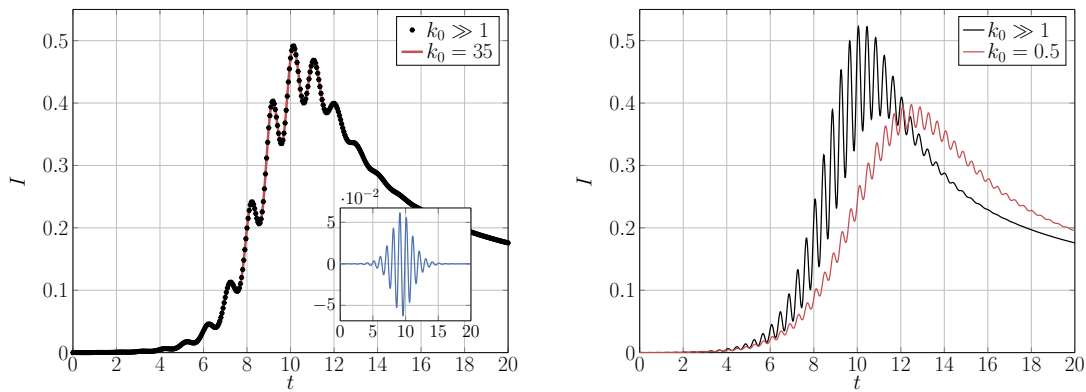
(A) ACV voltammogram for $\Delta\theta = 0.1$ and $\omega = 2\pi$. Inset shows the AC component.

(B) ACV voltammogram for $\Delta\theta = 0.1$ and $\omega = 5\pi$.

FIGURE 5. Voltammogram for ACV with $d = 3$ for different frequencies ω. The asymptotic formula for reversible reactions (25) is depicted in both plots as $k_0 \gg 1$. For the spatial discretisation a Chebyshev collocation with $N = 20$ is used and the timestep is $\Delta t = 10^{-4}$.

The agreement between the current derived from (25) and the numerics for moderate values of k_0 is, again, striking, see Figure 5a. If we, instead, consider a quasi-reversible reaction, then there is an observable difference, see Figure 5b. The ac component of the current becomes smaller in this case and we have the same shift in voltammogram as was observed for LSV, which could be anticipated from the specific form of the potential.

In analysing the ac component of the signal it has been observed both analytically [4] and numerically [6] that for reversible reactions the peak of the alternating current component scales linearly with $\sqrt{\omega}$ and $\Delta\theta$. These observations are confirmed by numerical simulations, see Figure 6 and 7. These depict the results of simulations with $N = 50$ and $\Delta t = 10^{-4}$. As noted by [6], one needs to choose Δt small enough so that we have enough timepoints to fully capture each cycle of the alternating current.

4.5. **Square wave voltammetry.** Another technique which tries to minimise the capacitive currents is the square wave voltammetry (SWV). In spirit it is very similar to ACV, but instead of adding a sinusoidal perturbation we superimpose a square wave to the signal. Just as for ACV we consider linear SWV, where the base dc signal is a linear sweep potential

$$(32) \qquad \theta(t) = \theta_0 + t + \Delta\theta(-1)^{\lfloor \omega t \rfloor}.$$
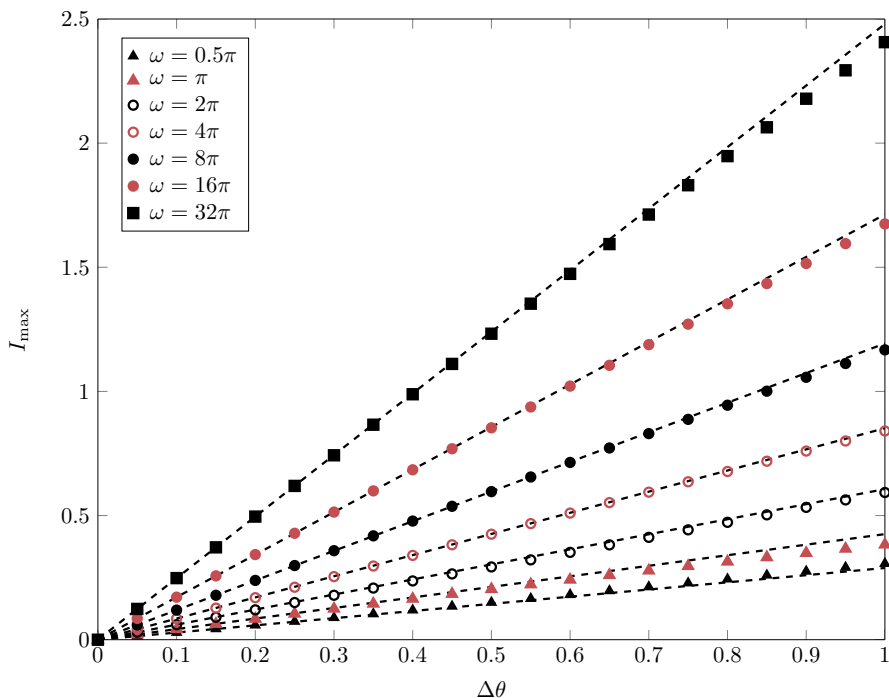
FIGURE 6. The peak ac current $I_{\max}$ as a function of the amplitude of the ac component of the potential $\Delta\theta$ for various ω. The reaction rate constant $k_0 = 35$. For a reasonable range of $\Delta\theta$ there exists a good linear fit as is shown by the dotted lines, closely resembling the results by Gavaghan & Bond [6].

4.5.1. *Numerical solution.* The potential for SWV contains jumps, which cannot be accurately described in a discretised manner. This will cause some issues, similar to the ones observed for chronoamperometry.

4.5.2. *Fourier analysis - harmonics.* Gavaghan et al. [7] inverstigated SWV for reversible reactions using Fourier analysis of the current. They observed that the signal is composed of the odd harmonics of the SWV frequency ω. This can be understood by looking at the actual potential in Fourier space. The square wave function can be expanded into its Fourier sine series to yield

$$(33) \qquad \theta(t) = \theta_0 + t + \frac{4\Delta\theta}{\pi} \sum_{k=1,3,\ldots}^{\infty} \frac{\sin(k\pi\omega t)}{k}.$$

The square wave is only composed of odd harmonics of ω. Note, however, that this merely suggests that we would observe the odd harmonics. It is in the case of ACV that the potential purely consists of a dc and an ω term, and that the signal is comprised of all harmonics.

This is clearly visible in Figure 8, where only the odd harmonics of $\omega = 2\pi$ are present in the power spectrum of the current. One can also see that the current exhibits spikes, due to the discontinuity in the potential as was anticipated. This discontinuities make very accurate results just around the potential switch difficult.

The Fourier transform contains more interesting information. As the zero frequency component is not interfering with the harmonics, we can single out the dc contribution. This is crudely done by applying a block filter, which zeroes all but the near surrounding of the zero frequency.
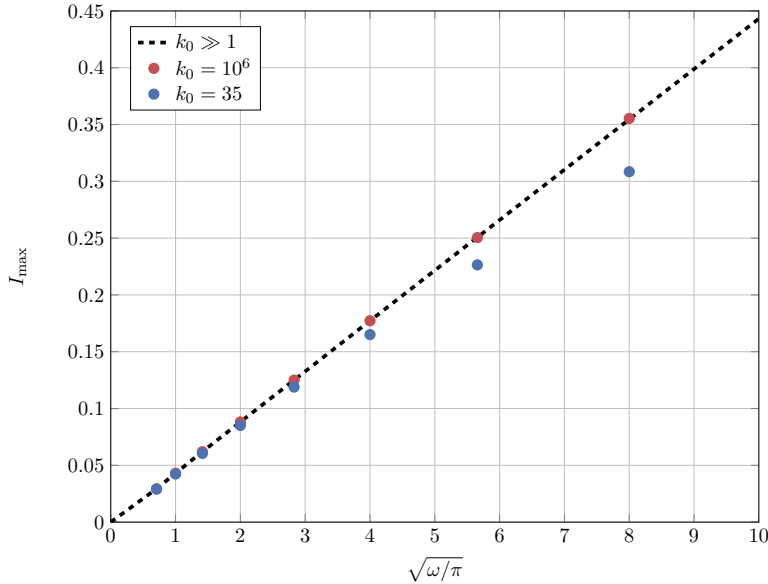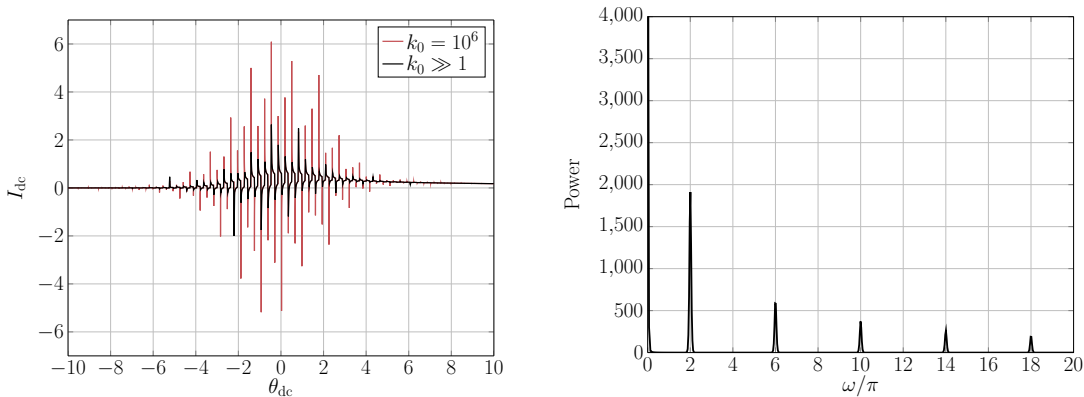
FIGURE 7. The peak ac current $I_{\max}$ as a function of the square root of the ac frequency ω for various k_0. The linear line is provided by the asymptotic formula for reversible reaction (25). The dots depict numerical results for $\omega = \pi/2, \pi, 2\pi, \ldots, 64\pi$. The linear relation is in agreement with the results by Gavaghan & Bond [6].

(A) SWV voltammogram for $\Delta\theta = 0.5$ and $\omega = 2\pi$ as a function of θ_{dc} (the LSV potential).

(B) Powerspectrum of the current of the SWV voltammogram in Figure 8a.

FIGURE 8. Voltammogram for SWV with $d = 2$. The asymptotic formula for reversible reactions (25) is depicted in Figure 8a as $k_0 \gg 1$. The power spectrum of the voltammogram is displayed in Figure 8b. Note that the amplitude of the dc component is $\sim 10^4$ and is ommited for clarity. For the spatial discretisation a Chebyshev collocation with $N = 50$ is used and the timestep is $\Delta t = 5 \cdot 10^{-5}$.

If we then take the inverse Fourier Transform of this filtered signal we retrieve the dc signal. Interestingly there is a qualitative change as the dc component develops two peaks as $\Delta\theta$ increases.

An explanation is offered by Oldham, Gavaghan & Bond [9]. The potential is a combination of two linear sweeps which are turned on alternatively. The two peaks originate from these two sweeps. They separate as $\Delta\theta$ increases, one towards the positive θ direction and one towards the negative.
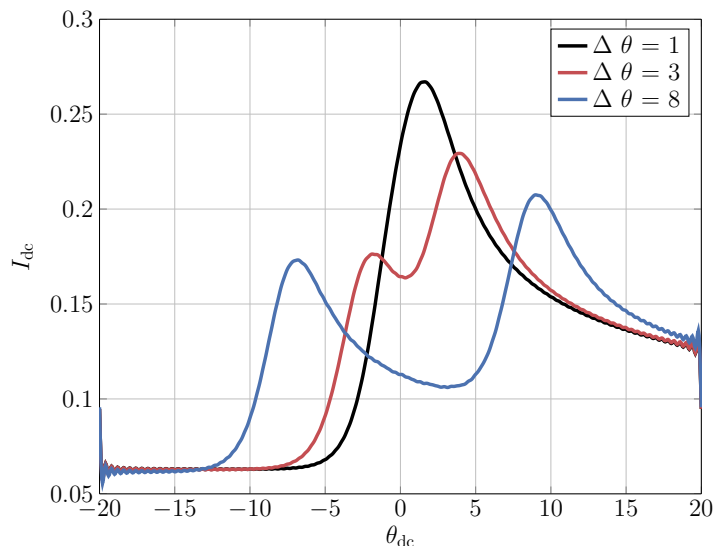

FIGURE 9. The dc current component for SWV as a function of θ_{dc} (the LSV potential). Model parameters are $d = 1$, $\omega = 4\pi$ and $k_0 = 10^6$. The results yield good agreement with Gavaghan et al. [7].

5. CONCLUSION

We derived a mathematical model for the dynamics of a single redox reaction, given by (5), at an electrode immersed in a liquid. Upon specification of the externally applied potential we could derive a closed set of equations. Five specific external potentials were considered in more detail, representing the following electrochemical techniques; chronoamperometry, linear sweep voltammetry, cyclic voltammetry, alternating current voltammetry and square wave voltammetry. A combination of analytical expressions in the case of reversible reactions and numerics in the case of (quasi)-reversible reactions provides a versatile way to explore common electrochemical problems.

The analysis set out in this paper could be easily extended in a few ways. Firstly we could look into the effect of more involved reaction mechanisms, as already mentioned when discussing cyclic voltammetry. Different electrode geometries, such as a disc or a heterogeneous surface, could be another generalisation of the results in this paper, which only discusses planar electrodes. This might require numerical simulations in two or three dimensions. The effect of chemical transport by means other than diffusion, such as convection, could also be considered.

Appendix A. Appendix

A.1. **Convergence rate numerics.** As we have an analytical solution in the chronoamperometry problem we can use this problem as a benchmark for the solver routines. We look for the $|| \cdot ||_\infty$ of the exact solution and the numerical solution. Note that because of the initial inconsistency it is expected that the error is initially $\mathcal{O}(1)$. We neglect this initial effect and look for the error after its contribution has decayed.

Firstly we fix $\Delta t = 10^{-6}$ and look at the effect of the number of spatial points for both methods, see Figure 10.
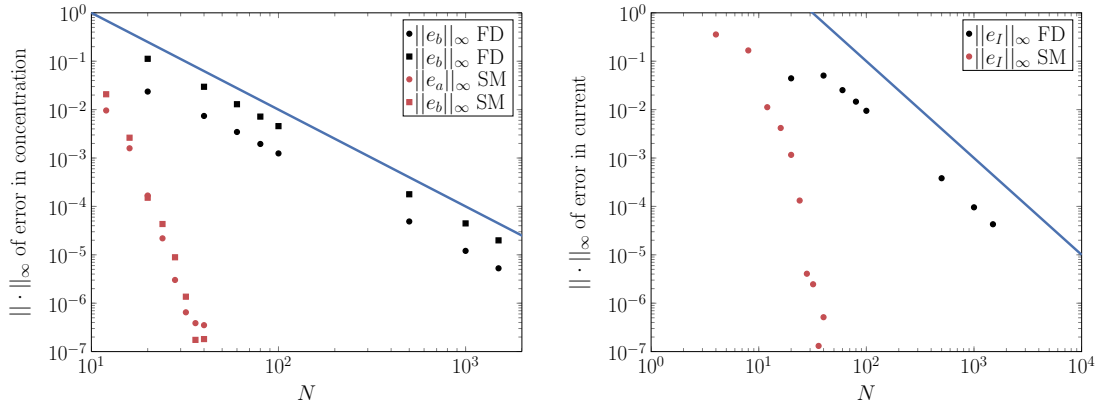
(A) Error in the numerical approximation of the concentration.

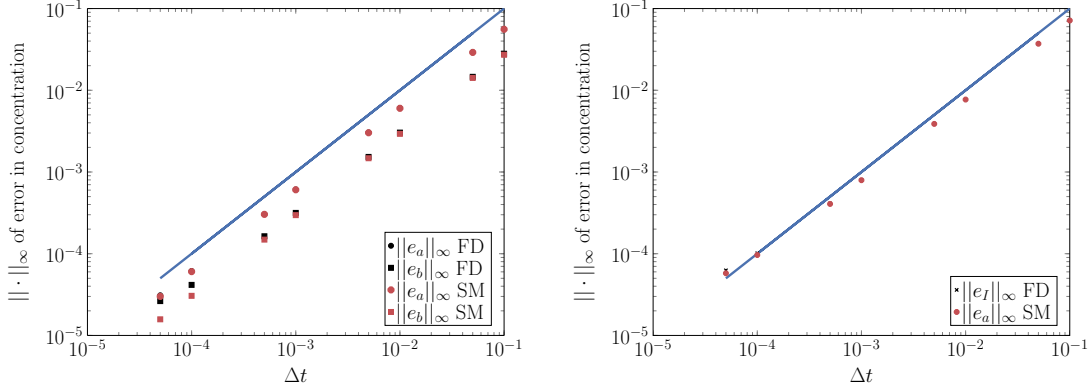(B) Error in the numerical approximation of the current.

FIGURE 10. Plot of the $|| \cdot ||_\infty$ numerical error of both the concentration and current for finite difference (FD) and the Chebyshev collocation (SM) as a function of the number of gridpoints N. A (blue) line with slope indicating quadratic convergence is plotted as a reference. We used timestep $\Delta t = 10^{-6}$, $d = 4$, final time $T = 1$ and $x^* = 30$.

One can see that the finite difference approximation indeed converges quadratically and the spectral method shows a much faster convergence. For the spectral method we see that for roughly $N = 30$ we hit a barrier at $\sim 10^{-6}$. This is due to the error in the time-stepping caused by the implicit Euler scheme.

We can also fix the number of spatial grid points and look at the error as a function of Δt, see Figure 11. Again we observe good agreement with the theory, which predicts a linear convergence rate, regardless of the spatial discretisation used.

A.2. **Similarity solution chronoamperometry.** We seek a similarity solution of the form $a(x,t) = f(\eta)$ and $b(x,t) = g(\eta)$ with $\eta = x/\sqrt{t}$. The diffusion equations in the new similarity coordinate become

$$(34) \qquad -\frac{1}{2}\eta f'(\eta) = f''(\eta), \qquad -\frac{1}{2}\eta g'(\eta) = dg''(\eta),$$

(A) Error in the numerical approximation of the concentration.

(B) Error in the numerical approximation of the current.

FIGURE 11. Plot of the $||\cdot||_\infty$ numerical error of both the concentration and current for finite difference (FD) and the Chebyshev collocation (SM) as a function of the timestep Δt. A (blue) line with slope indicating linear convergence is plotted as a reference. We used timestep $N_{\mathrm{FD}} = 2000$, $N_{\mathrm{SM}} = 30$, $d = 4$, final time $T = 1$ and $x^* = 30$.

with $' = \frac{d}{d\eta}$. These ODEs for f and g can be explicitly integrated to give

$$(35) \qquad f(\eta) = c_1 \mathrm{erf}(\eta/2) + c_2, \qquad g(\eta) = c_3 \mathrm{erf}(\eta/2\sqrt{d}) + c_4.$$

The integration constants c_i are determined by the boundary conditions (12d-12e,20)

$$(36) \qquad 1 = c_1 + c_2, \quad 0 = c_3 + c_4, \quad c_2 = c_4 e^{-\theta}, \quad c_1 = -\sqrt{d}c_3.$$

Note that in order to have a valid similarity solution we need that $\theta =$ constant to make the boundary conditions consistent with the similarity variable. Solving for the integration constants one finds (21a,21b).

A.3. **Current for reversible reactions.** We consider the problem (12a-12g), where instead of (12e) we work with the Nernst-equation (20) at the electrode-liquid interface because of the reversibility of the reaction $(k_0 \gg 1)$.

Now we take the Laplace transform of a and b with respect to t

$$(37) \qquad A(x, s) = \mathcal{L}[a(x, t); t], \qquad B(x, s) = \mathcal{L}[b(x, t); t].$$

We use the boundary conditions and the properties of the Laplace transform to find

$$(38) \qquad \mathcal{L}[a_t(x, t); t] = sA(x, s) - 1, \qquad \mathcal{L}[b_t(x, t); t] = sB(x, s).$$

The diffusion equations for a and b consequently transform to

$$(39a) \qquad \frac{\partial^2 A}{\partial x^2} = sA(x, s) - 1,$$

$$(39b) \qquad d\frac{\partial^2 B}{\partial x^2} = sB(x, s),$$

which is supplemented by Laplace transforms of the boundary conditions

$$(40a) \qquad\qquad A \to \frac{1}{s}, \; B \to 0, \qquad \text{as } x \to \infty,$$

$$(40b) \qquad\qquad \frac{\partial A}{\partial x} + d\frac{\partial B}{\partial x} = 0, \qquad \text{at } x = 0,$$

$$(40c) \qquad\qquad A(0, s) = \mathcal{L}\left[e^{-\theta(t)} b(0, t) \right].$$

These equations can be solved and this yields

$$(41) \qquad A(x, s) = \left(A(0, s) - \frac{1}{s} \right) e^{-\sqrt{s}x} + \frac{1}{s}, \qquad B(x, s) = B(0, s)e^{-\sqrt{s}x/\sqrt{d}}.$$

Note that (40b,41) together with (40c) gives

$$(42) \qquad -\sqrt{s}\left(\mathcal{L}\left[e^{-\theta(t)} b(0, t) \right] - \frac{1}{s} \right) = \left.\frac{\partial A}{\partial x}\right|_{x=0} = -d\left.\frac{\partial B}{\partial x}\right|_{x=0} = \sqrt{sd}\mathcal{L}\left[b(0, t) \right].$$

This can be solved for $b(0, t)$ (and thus $a(0, t)$ as well) by taking the inverse Laplace transform on both side and using linearity

$$(43) \qquad\qquad b(0, t) = \frac{e^{\theta(t)}}{\sqrt{d}e^{\theta(t)} + 1}, \qquad a(0, t) = \frac{1}{\sqrt{d}e^{\theta(t)} + 1},$$

generalising for non-constant θ the chronoamperometry boundary conditions.

Finally, since $I(t) = a_x(0, t)$ we find upon taking its Laplace transform

$$(44) \qquad\qquad \mathcal{L}[I(t)] = \left.\frac{\partial A}{\partial x}\right|_{x=0} = \sqrt{sd}\mathcal{L}\left[b(0, t) \right].$$

This then yields that

$$(45) \qquad\qquad \frac{\sqrt{\pi}}{\sqrt{s}}\mathcal{L}[I(t)] = \sqrt{d\pi}\mathcal{L}\left[b(0, t) \right],$$

which we can transform back to original coordinates by taking the inverse Laplace transform. Note then that $\mathcal{L}(1/\sqrt{t}) = \sqrt{\pi}/\sqrt{s}$. Upon using $b(0, t)$ and using the convolution theorem for the Laplace transform this gives

$$(46) \qquad\qquad \frac{\sqrt{d\pi}e^{\theta(t)}}{\sqrt{d}e^{\theta(t)} + 1} = I(t) * \mathcal{L}^{-1}\left[\frac{\sqrt{\pi}}{\sqrt{s}} \right] = I(t) * \frac{1}{\sqrt{t}}.$$

This finally yields the desired implicit relation for the current

$$(47) \qquad\qquad F(t) = \frac{\sqrt{d\pi}}{\sqrt{d} + e^{-\theta(t)}} = \int_0^t \frac{I(\tau)}{\sqrt{t - \tau}} \, d\tau.$$

A.3.1. *Numerical approximation integral.* Two ways are proposed to circumvent the divergence of the integrand. Firstly we can use an integration by parts to find

$$F(t) = \int_0^t \frac{I(\tau)}{\sqrt{t - \tau}} \, d\tau = -2I(\tau)\sqrt{t - \tau}\Big|_0^t + 2\int_0^t I'(\tau)\sqrt{t - \tau} \, d\tau,$$

$$= -2I(0)\sqrt{t} + 2\int_0^t I'(\tau)\sqrt{t - \tau} \, d\tau,$$

$$(48) \qquad\qquad = 2\int_0^t I'(\tau)\sqrt{t - \tau} \, d\tau.$$

This removed the singularity of the integrand at the cost of replacing $I(t)$ by its time-derivative. Another method accomplishes a similar result, but without replacing $I(t)$ by a derivative. This is achieved by integrating the implicit current integral

$$
\begin{aligned}
G(t) = \int_0^t F(s)\, ds &= \int_0^t \int_0^s \frac{I(\tau)}{\sqrt{s-\tau}}\, d\tau\, ds, \\
&= \int_0^t \int_\tau^t \frac{I(\tau)}{\sqrt{s-\tau}}\, ds\, d\tau, \\
&= 2\int_0^t I(\tau)\sqrt{t-\tau}\, d\tau.
\end{aligned}
$$
(49)

As mentioned in the paper the numerical approximation relies on approximation of integrals of the form

$$
(50) \qquad \int_{t_i}^{t_{i+1}} I'(\tau)\sqrt{t-\tau}\, d\tau, \qquad \int_{t_i}^{t_{i+1}} I(\tau)\sqrt{t-\tau}\, d\tau.
$$

Here we will only describe four closely related quadrature methods.

The first method, applicable to both integrals, is the midpoint-approximation. This method approximates the integral by the area of a rectangle whose height is determined by the integrand value at the midpoint of the integration domain

$$
(51a) \qquad \int_{t_i}^{t_{i+1}} I'(\tau)\sqrt{n\Delta t-\tau}\, d\tau \approx \Delta t I'(t_{i+\frac{1}{2}})\sqrt{\Delta t}\sqrt{n-i-\frac{1}{2}} \approx (I_{i+1}-I_i)\sqrt{n-i-\frac{1}{2}}\sqrt{\Delta t},
$$

$$
(51b) \qquad \int_{t_i}^{t_{i+1}} I(\tau)\sqrt{n\Delta t-\tau}\, d\tau \approx \Delta t I(t_{i+\frac{1}{2}})\sqrt{\Delta t}\sqrt{n-i-\frac{1}{2}}
$$

where we have used $I'(t_{i+\frac{1}{2}}) \approx (I_{i+1}-I_i)/\Delta t$, the central approximation of the first derivative.

The other methods use a partial midpoint method, namely assuming that $I'(\tau) = I'(t_{i+\frac{1}{2}})$ over the integration, to give

$$
(52) \qquad \int_{t_i}^{t_{i+1}} I'(\tau)\sqrt{n\Delta t-\tau}\, d\tau \approx I'(t_{i+\frac{1}{2}}) \int_{t_i}^{t_{i+1}} \sqrt{n\Delta t-\tau}\, d\tau.
$$

The last integral can be either calculated exactly to yield

$$
(53) \qquad \int_{t_i}^{t_{i+1}} I'(\tau)\sqrt{n\Delta t-\tau}\, d\tau \approx \frac{2}{3}(I_{i+1}-I_i)\sqrt{\Delta t}\left((n-i)^{\frac{3}{2}}-(n-i-1)^{\frac{3}{2}}\right),
$$

or approximated by use of the trapezium rule

$$
(54) \qquad \int_{t_i}^{t_{i+1}} I'(\tau)\sqrt{n\Delta t-\tau}\, d\tau \approx \frac{1}{2}(I_{i+1}-I_i)\sqrt{\Delta t}\left((n-i-1)^{\frac{1}{2}}+(n-i)^{\frac{1}{2}}\right).
$$

We note that all approximations are indeed of the form (28) for different constants p_i. This yields the approximations

$$
(55a) \qquad F(n\Delta t) \approx 2\sqrt{\Delta t}\sum_{i=0}^{n-1} p_i(I_{i+1}-I_i) = 2\sqrt{\Delta t}\left(p_{n-1}I_n + \sum_{i=1}^{n-1}(p_{i-1}-p_i)I_i - p_0 I_0\right),
$$

$$
(55b) \qquad G(n\Delta t) \approx 2\Delta t\sqrt{\Delta t}\sum_{i=0}^{n-1}\left(\sqrt{n-i-\frac{1}{2}}\right)I(t_{i+\frac{1}{2}}).
$$

This can be rewritten to find I_n as a function of the current at the previous times

$$
(56a) \qquad I_n \approx \frac{1}{p_{n-1}} \left(\frac{F(n\Delta t)}{2\sqrt{\Delta t}} + p_0 I_0 - \sum_{i=1}^{n-1} (p_{i-1} - p_i) I_i \right),
$$

$$
(56b) \qquad I_{n-\frac{1}{2}} \approx \sqrt{2} \left(\frac{G(n\Delta t)}{2\Delta t \sqrt{\Delta t}} + \sum_{i=0}^{n-2} \left(\sqrt{n - i - \frac{1}{2}} \right) I_{i+\frac{1}{2}} \right).
$$

A final note can be made on the cost of the approximation. It appears that the methods that work with $F(t)$ instead of $G(t)$ are more advantageous, as they do not require an extra integration. In the case of LSV however the integral $G(t)$ can be calculated explicitly

$$
(57) \qquad G(t) = \int_0^t F(s)\, \mathrm{d}s = \int_0^t \frac{\sqrt{d\pi}}{\sqrt{d} + e^{-\theta_0 - s}}\, \mathrm{d}s = \sqrt{\pi} \log \left(\frac{e^{-\theta_0} + e^t \sqrt{d}}{e^{-\theta_0} + \sqrt{d}} \right),
$$

which puts the method on equal scale with the other methods.

The methods could be slow if implemented naively, where at every iteration we need to compute an increasing number of coefficients and sum those. A significant speed-up can be achieved if these coefficients are initially vectorised so that we only have to compute them once. We then can code the summation over all previous I_i as a vector-vector product so that the cost of every new time step is just roughly a vector-vector product.

References

1. Bard, A. J. & Faulkner, L. R. *Electrochemical Methods: Fundamentals and Applications* (Wiley, 2000).
2. Butler, J. A. V. Studies in heterogeneous equilibria. Part II. The kinetic interpretation of the nernst theory of electromotive force. *Transactions of the Faraday Society* **19,** 729 (1924).
3. Compton, R. G., Laborda, E. & Ward, K. *Understanding Voltammetry* (Imperial College Press, 2014).
4. Engblom, S. O., Myland, J. C. & Oldham, K. B. Must ac voltammetry employ small signals? *Journal of Electroanalytical Chemistry* **480,** 120–132 (2000).
5. Erdey-Gruz, T. & Volmer, M. Zur theorie der wasserstoffüberspannung. *Z. Phys. Chem. A* **150,** 203 (1930).
6. Gavaghan, D. & Bond, A. A complete numerical simulation of the techniques of alternating current linear sweep and cyclic voltammetry: analysis of a reversible process by conventional and fast Fourier transform methods. *Journal of Electroanalytical Chemistry* **480,** 133–149 (2000).
7. Gavaghan, D., Elton, D., Oldham, K. & Bond, A. Analysis of ramped square-wave voltammetry in the frequency domain. *Journal of Electroanalytical Chemistry* **512,** 1–15 (2001).
8. Hundsdorfer, W. & Verwer, J. G. *Numerical Solution of Time-Dependent Advection-Diffusion-Reaction Equations* (Springer Science & Business Media, 2003).
9. Oldham, K. B., Gavaghan, D. J. & Bond, A. M. A Full Analytic Treatment of Reversible Linear-Scan Voltammetry with Square-Wave Modulation. *The Journal of Physical Chemistry B* **106,** 152–157 (2002).
10. Trefethen, L. N. *Spectral Methods in MATLAB* (Society for Industrial and Applied Mathematics, 2000).